Turbulence, Condensation, and Liquid Water Transport in Numerically Simulated Nonprecipitating Stratocumulus Clouds

SHOUPING WANG

Naval Research Laboratory, Monterey, California

QING WANG

Naval Postgraduate School, Monterey, California

GRAHAM FEINGOLD

NOAA/Environmental Technology Laboratory, Boulder, Colorado

(Manuscript received 10 December 2001, in final form 26 June 2002)

ABSTRACT

Condensation and turbulent liquid water transport in stratocumulus clouds involve complicated interactions between turbulence dynamics and cloud microphysical processes, and play essential roles in defining the cloud structure. This work aims at understanding this dynamical–microphysical interaction and providing information necessary for parameterizations of the ensemble mean condensation rate and turbulent fluxes of liquid water variables in a coupled turbulence–microphysics model. The approach is to simulate nonprecipitating stratocumulus clouds with a coupled large eddy simulation and an explicit bin-microphysical model, and then perform a budget analysis for four liquid water variables: mean liquid water content, turbulent liquid water flux, mean cloud droplet number concentration, and the number density flux. The results show that the turbulence contribution to the mean condensation rate comes from covariance of the integral cloud droplet radius and supersaturation, which enhances condensation in turbulent updrafts and reduces evaporation in the downdrafts. Turbulent liquid water flux results from a close balance between turbulence dynamics and microphysical processes. Consequently, the flux can be parameterized in terms of the common diffusive downgradient formulation, fluxes of conservative thermodynamic variables, the turbulence mixing timescale, and the condensation timescale, which is determined by the droplet spectrum. The results also suggest that the condensation timescale regulates the turbulence fields, as does the number concentration, because it affects the condensation fluctuation, which is highly correlated with the turbulence vertical motion. A saturation adjustment cloud model, which diagnoses liquid water content at its equilibrium level, instantly condenses (evaporates) all available water vapor (liquid water) surplus. Consequently, there is likely to be a systematic difference between the turbulence field resolved with this type of model and that with a supersaturation-based cloud scheme for which a finite condensation timescale applies.

1. Introduction

It has been recognized that microphysics may play an important role in regulating dynamics of stratocumulus clouds and their impact on the weather from local to climate scales. These roles include the so-called ''indirect aerosol effects'' as discussed by Twomey (1977) and Albrecht (1989), as well as the precipitation effects that may change the stability in stratocumulus cloud-topped boundary layers (e.g., Paluch and Lenschow 1991; Wang and Wang 1994; Stevens et al. 1998b). For this reason, efforts have increasingly focused on representing detailed microphysics in a dynamic framework of stratocumulus clouds to understand physical processes and to predict the impacts on large-scale meteorological fields. Large eddy simulation (LES) and turbulence closure models are two commonly used dynamic frameworks for stratocumulus clouds. For example, Feingold et al. (1994) and Bott et al. (1996), respectively, implemented explicit bin cloud microphysics representations in an LES and turbulence closure model.

A successful dynamical–microphysical model must include some basic coupling between turbulence dynamics and microphysical processes. It is well known that vertical motion strongly affects cloud droplet activation, condensation, and liquid water transport (e.g., Stevens et al. 1998a). An excess of water vapor is pro-

Corresponding author address: Shouping Wang, Naval Research Laboratory, 7 Grace Hopper Ave., MS2, Monterey, CA 94943.
E-mail: wang@nrlmry.navy.mil

duced at the cloud base by turbulent updrafts and initiates droplet activation. In the turbulent updrafts, the condensational latent heat released from rapid droplet growth further enhances upward motion; while in the downdrafts, evaporation in the subsaturated environment strengthens the downward motion. It is clear that in this process condensation/evaporation (CE) is strongly controlled by turbulent vertical motion and liquid water is not conserved during turbulent ascent and descent. In the LES framework, this coupling is relatively straightforward, because the stochastic large eddies that contain most of the energy are explicitly resolved. Therefore, a bin-resolved cloud microphysical model that generates supersaturation and activates and grows droplets based on resolved vertical motions can be directly implemented in an LES model without major parameterization of the turbulence–microphysics coupling (e.g., Feingold et al. 1994; Kogan et al. 1995).

Microphysical representation in a turbulence-parameterized model is significantly more complex; because the turbulence dynamics in such models is parameterized, the basic turbulence–microphysics coupling must be explicitly parameterized too. A key question in this parameterization is how the ensemble mean CE rate and the turbulent liquid water (and droplet number) flux should be related to the mean and turbulence fields. Stevens et al. (1998a) discussed this issue in detail and pointed out that the interaction between turbulence and microphysics is critical in developing an explicit bin microphysical model for a turbulence parameterization.

Turbulence–microphysics interaction has been a subject of many studies (e.g., Telford and Chai 1980; Cooper 1989). These studies have, however, primarily focused on turbulence effects on the broadening of the cloud droplet size spectra, rather than on the turbulence–microphysical statistical quantities and their parameterizations. Khvorostyanov and Curry (1999) developed a stochastic condensation theory, which includes a treatment of the covariance of velocity and liquid water variables based on the turbulence statistical theory and characteristics of the turbulence and the droplet size spectra.

A coupled LES–bin-microphysical (LES-BM) model explicitly resolves both the large eddy turbulence field and the associated cloud droplet spectrum, and thus can be used to provide detailed and quantitative information on some basic turbulence–microphysics coupling issues. Since our focus is on statistical quantities, the turbulence budget analysis is particularly useful because this type of analysis (e.g., Moeng and Wyngaard 1986) may provide not only the physical understanding, but also some implications for the parameterization approaches.

In this work, the budgets of four liquid water variables will be derived in terms of bulk cloud mean and turbulence fields. These variables are mean liquid water content, turbulent liquid water flux, mean cloud droplet number concentration, and the number density flux, denoted by $\overline{q_l}$, $\overline{w'q_l'}$, $\overline{N}$, and $\overline{w'N'}$, respectively. An LES-BM model is used to simulate a stratocumulus-capped boundary layer. Then these budgets are analyzed based on the simulations. Our main questions are: How does the turbulence interact with the microphysics to produce the ensemble mean CE rate and the fluxes? And how can one parameterize them?

2. LES-BM model

The LES-BM model used in this study is very similar to that of Stevens et al. (1996a). A detailed description and a comprehensive evaluation and description of the LES code is given by Stevens et al. (1999). Of relevance to this study is the fact that monotone operators are used for scalar advection (following Zalesak 1979) and Deardorff's prognostic turbulent kinetic energy (TKE) technique is used for the subgrid-scale (SGS) model (Deardorff 1980). At the surface, Monin–Obukhov similarity theory provides the surface fluxes based on assumed sea surface temperature and the predicted winds, temperature, and moisture at the first level. At the top of the domain, a constant gradient condition is applied to all scalar variables and a free slip for momentum. The lateral boundary conditions are periodic.

The bin microphysical model was developed by Feingold et al. (1994), and was also described in detail in Stevens et al. (1996a). Briefly, the droplet size spectrum is divided into 25 size bins in which both the droplet mass and number concentration are predicted. The diagnostic activation scheme is based on the cumulative method discussed by Clark (1973) where the number of droplets in the first bin is incremented by the difference between the number of cloud condensation nuclei (CCN) that should be activated at the calculated supersaturation, and the local droplet number. The aerosol spectrum is assumed to follow a constant lognormal distribution with a total aerosol concentration N_a.

Our focus is on the basic interaction among turbulence, CE rates, and liquid water fluxes. Particularly, response of the turbulence to the different CE timescales will be studied. Therefore, the processes of droplet coalescence–collection and sedimentation (''drizzle processes'') are not represented in the first three simulations so as to isolate the targeted coupled system and facilitate comparisons. Drizzle is included in two other simulations for evaluation of our results.

The four-stream radiation parameterization developed by Fu et al. (1995) is used to calculate radiative cooling rates. To better focus on our objective, we purposely disconnect the link between the predicted droplet spectrum and the radiation by specifying the droplet number mixing ratio at 100 mg^{-1} for the longwave, and by not simulating shortwave radiation. For the stratocumulus case here, the model uses 60×60 grid points with uniform spacing $\Delta x = \Delta y = 50$ m in the horizontal; there are 76 grid points in the vertical with a minimum spacing of 5 m within the inversion and 25 m below

the inversion to span a 3 km × 3 km × 2.1 km domain. The time step is 1.5 s.

3. Budget equations

One of our objectives is to derive a method of parameterization for the liquid water variables. Therefore, we require that the budget equations be expressed in terms of the commonly used bulk cloud variables such as q_l and N (instead of the droplet mass and number in each bin, or the radius), although the simulations are performed with the full bin microphysical model. The starting point for the budgets is the governing equation for the time rate of change of the droplet number density due to CE (e.g., Clark 1973):

$$\left[\frac{\partial n(r)}{\partial t}\right]_{\text{CE}} = -\frac{\partial}{\partial r}\left[\frac{n(r)G(T, p)S}{r}\right], \tag{1}$$

where $n(r)$ is the droplet number density with radius r, $n(r)dr$ the droplet number per unit air mass in the interval $(r, r + dr)$, $G(T, p)$ a function of temperature and pressure, and S the surplus vapor ($S = q_v - q_s$). By definition, $N = \int_0^\infty n(r)\, dr$. The third moment integration gives the local instantaneous CE rate

$$\left(\frac{\partial q_l}{\partial t}\right)_{\text{CE}} = -\rho_l \frac{4}{3}\int_0^\infty r^3 \frac{\partial}{\partial r}\left(\frac{nGS}{r}\right) dr = 4\pi G \rho_l R S, \tag{2}$$

where R is the integrated radius [$\int_0^\infty rn(r)\, dr$], and ρ_l is the liquid water density. Applying the Reynolds averaging operation gives the following ensemble mean CE rate:

$$\left(\frac{\partial \overline{q}_l}{\partial t}\right)_{\text{CE}} \cong 4\pi G(\overline{T}, \overline{p})\rho_l(\overline{R}\,\overline{S} + \overline{R'S'}), \tag{3}$$

where $\overline{G}(T, p) \cong G(\overline{T}, \overline{p})$ and the correlation between G and others are neglected due to its relatively weak dependence on T and p, which has been confirmed in the LES-BM model simulations (see appendix A). We need to express $\overline{R}$ and R' in terms of $\overline{q}_l$, $\overline{N}$, q_l', and N', which requires a specific distribution. Feingold et al. (1998) successfully used lognormal distribution functions to parameterize the droplet and rain spectra for stratocumulus modeling. Based on this distribution function, the integral radius can be determined by

$$R(q_l, N, a) = \frac{e^{(-\ln^2 a)}}{(4/3\pi\rho_l)^{1/3}}(q_l N^2)^{1/3}, \tag{4}$$

where a is the geometric standard deviation and is specified as a constant. If (4) is expanded at $(\overline{q}_l, \overline{N})$ in a Taylor series and only the first-order terms are retained,

$$R' \cong \frac{\overline{R}}{3}\left(\frac{q_l'}{\overline{q}_l} + \frac{2N'}{\overline{N}}\right), \tag{5}$$

where

$$\overline{R} = R(\overline{q}_l, \overline{N}, a).$$

Combining (3), (4), and (5), and including turbulence flux divergence and large-scale subsidence terms, we obtain the $\overline{q}_l$ budget:

$$\frac{\partial \overline{q}_l}{\partial t} = \underbrace{-\overline{w}\frac{\partial \overline{q}_l}{\partial z}}_{L} \underbrace{- \frac{\partial(\overline{w'q_l'} + \overline{\langle w''q_l''\rangle})}{\partial z}}_{T} + \Bigg[\underbrace{b\overline{R}\,\overline{S}}_{1} + \underbrace{\frac{b\overline{R}}{3}\frac{\overline{q_l'S'}}{\overline{q}_l}}_{2} + \underbrace{\frac{b\overline{R}}{3}\frac{2\overline{N'S'}}{\overline{N}}}_{3} + \underbrace{\overline{A}_C}_{4}\Bigg], \tag{6}$$

where $b \equiv 4\pi\overline{G}\rho_l$, the double prime "″" represents SGS fluctuation, and angle brackets are a grid-volume averaging operator. The first two terms are the large-scale subsidence (L) and divergence of the turbulent flux (T), respectively. The four terms in the square brackets—that is, mean saturation, two turbulence covariance terms, and activation—are denoted by the numbers 1–4, respectively. The liquid water flux budget, derived in appendix B, is written as

$$\frac{\partial \overline{w'q_l'}}{\partial t} = \underbrace{-\frac{\partial \overline{w'w'q_l'}}{\partial z}}_{T} \underbrace{- \overline{w'^2}\frac{\partial \overline{q}_l}{\partial z}}_{G} + \underbrace{\frac{g}{\theta_0}\overline{\theta_v' q_l'}}_{B} \underbrace{- \frac{1}{\rho_0}\overline{q_l'\frac{\partial p'}{\partial z}}}_{P} \underbrace{- \left(\overline{w'\frac{\partial \tau_{li}'}{\partial x_i}} + \overline{q_l'\frac{\partial \tau_{zi}'}{\partial x_i}}\right)}_{\text{SGS}} + \Bigg[\underbrace{b\overline{R}\,\overline{w'S'}}_{1} + \underbrace{\frac{b\overline{R}\,\overline{S}}{3}\left(\frac{\overline{wq_l'}}{\overline{q}_l} + \frac{2\overline{w'N'}}{\overline{N}}\right)}_{2} + \underbrace{\frac{b\overline{R}}{3}\left(\frac{\overline{w'q_l'S'}}{\overline{q}_l} + \frac{2\overline{w'N'S'}}{\overline{N}}\right)}_{3} + \underbrace{\overline{w'A_c'}}_{4}\Bigg]. \tag{7}$$

The various terms are flux divergence (T); mean gradient production (G); buoyancy production (B); pressure perturbation (P); SGS term (SGS); and microphysical terms (in the square brackets), which are water vapor surplus flux, second-order covariance, third-order covariance, and activation flux, denoted by the corresponding numbers under (7).

The budgets of $\overline{N}$ and $\overline{w'N'}$ can be written as

TABLE 1. Simulation conditions and procedures (CE means that only activation, and condensation/evaporation are considered; drizzle means that all BM processes are included.)

Simulations	0–3 h	3–6 h	q_t above cloud
S1	LES-SA	LES-BM (CE) and CCN = 100 mg^{-1}	4.5 g kg^{-1}
S2	LES-SA	LES-BM (CE) and CCN = 1000 mg^{-1}	4.5 g kg^{-1}
S3	LES-SA	LES-SA	4.5 g kg^{-1}
S4	LES-SA	LES-BM (Drizzle), CCN = 100 mg^{-1}	4.5 g kg^{-1}
S5	LES-SA	LES-BM (Drizzle), CCN = 100 mg^{-1}	6.5 g kg^{-1}

$$\frac{\partial \overline{N}}{\partial t} = \underbrace{-\overline{w}\frac{\partial \overline{N}}{\partial z}}_{L} \underbrace{-\frac{\partial(\overline{w'N'} + \overline{\langle w''N''\rangle})}{\partial z}}_{T} + [\underbrace{\overline{A}_N}_{A} + \underbrace{\overline{E}_N}_{E}], \quad \text{and} \tag{8}$$

$$\frac{\partial \overline{w'N'}}{\partial t} = \underbrace{-\frac{\partial \overline{w'w'N'}}{\partial z}}_{T} \underbrace{-\overline{w'^2}\frac{\partial \overline{N}}{\partial z}}_{G} + \underbrace{\frac{g}{\theta_0}\overline{\theta_v' N'}}_{B} \underbrace{-\frac{1}{\rho_0}\overline{N'\frac{\partial p'}{\partial z}}}_{P} \underbrace{-\left(\overline{w'\frac{\partial \tau_{Ni}'}{\partial x_i}} + \overline{N'\frac{\partial \tau_{zi}'}{\partial x_i}}\right)}_{\text{SGS}} + [\underbrace{\overline{w'A_N'}}_{A} + \underbrace{\overline{w'E_N'}}_{E}], \tag{9}$$

where A_N and E_N are droplet number activation and evaporation rates. Due to the complexity of the activation and evaporation formulations, no attempts have been made to explicitly express $\overline{w'A_N'}$ and $\overline{w'E_N'}$ in terms of the mean and turbulence fields. The letters "A" and "E" under the equations represent activation and evaporation related processes, respectively, in the budgets, while other letters have similar meaning to those for $\overline{q_l}$ and $\overline{w'q_l'}$ budgets.

4. Stratocumulus cloud case

The San Nicolas Island sounding composited by Albrecht et al. (1995) from observations taken during the First International Satellite Cloud Climatology Project (ISCCP) Regional Experiment (FIRE) is used as a basis for the model initialization. A LES simulation with the sounding by Wang and Stevens (2000) showed that the modeled liquid water mixing ratio is relatively large; the maximum is 0.61 g kg^{-1} compared with 0.1~0.4 g kg^{-1} obtained by many other observations (e.g., Paluch and Lenschow 1991). Therefore, we intentionally reduce the moisture above the inversion from 6.5 g kg^{-1} to 4.5 g kg^{-1}, which is more in line with other observations (e.g., Paluch and Lenschow 1991; Lilly 1968), for the first four simulations, but still use 6.5 g kg^{-1} for the fifth simulation that includes drizzle. In addition, the constant sea surface temperature and the large-scale divergence is specified to be 288.8 K (Albrecht et al. 1995) and 6×10^{-6} s^{-1}, respectively. We emphasize that the specification of these large-scale conditions does not have any qualitative impact on our results as long as a radiatively driven stratocumulus-topped boundary layer is simulated. The model is first run for 3 h with the saturation adjustment procedure, then run with the bin-microphysical model for the next 3 h until a quasi steady state is achieved. All the turbulence and microphysics statistics are calculated and averaged over the last hour of the simulation with a sample interval of 9 s. Five simulations (S1–S5) are performed and the procedures are shown in Table 1.

5. Cloud water budgets

For the budget study, the results of S1 are analyzed. First, the general characteristics of simulated clouds are presented, and then the four cloud water budgets [(6)–(9)] are discussed. A classic well-mixed cloud-topped boundary layer is simulated with some mean and turbulence statistics displayed in Figs. 1a–c, which are consistent with our expectations and past experience. Figures 1d–f show profiles of the five cloud variables ($\overline{q_l}$, $\overline{w'q_l'}$, $\overline{N}$, $\overline{w'N'}$, and $\overline{r}_e$), which are in general agreement with other modeling studies (e.g., Stevens et al. 1996a) and observations (e.g., Nicholls 1984). Nonetheless, several important features are worth mentioning. The number concentration $\overline{N}$ is relatively constant within the cloud, which, together with the linear increase of $\overline{q_l}$, leads to an approximate increase of $\overline{r}_e$ with $z^{1/3}$. The liquid water flux $\overline{w'q_l'}$ is weakly negative at the cloud base, increases rapidly with height, and becomes positive for most of the cloud layer. The droplet number flux $\overline{w'N'}$ increases rapidly from a negative value to the maximum, and then decreases with height. The negative values of $\overline{w'q_l'}$ and $\overline{w'N'}$ at the cloud base result from the downward turbulent transport of the cloud droplets, leading to larger q_l and N in the downdrafts than those in the updrafts at those levels.

a. The q_l budget

An excellent balance exists between the flux divergence (including both resolved and SGS fluxes) and the condensation terms, while the subsidence advection term is negligibly small (Fig. 2a). Between 500 and 580 m near the cloud base (~530 m), the net evaporation is compensated by the flux convergence as shown in Fig. 2a. This evaporation and the negative liquid water

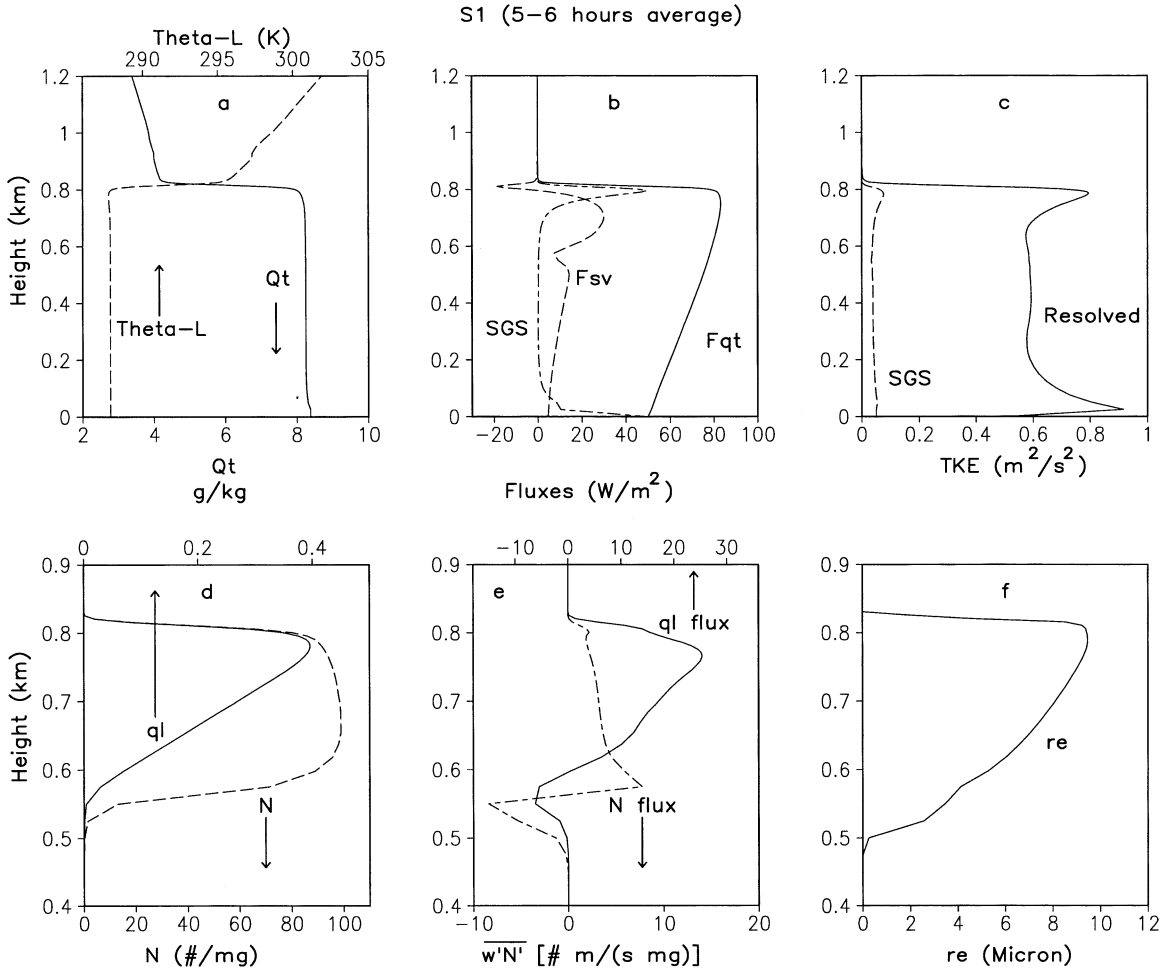

FIG. 1. Synopsis of some mean and turbulence variables from the S1 simulation: (a) $\overline{q}_l$ (solid) and $\overline{\theta}_l$ (dashed); (b) total $\rho_0 L\overline{w'q_t'}$ (solid), $\rho_0 L\overline{w'\theta_v'}$ (dashed), $\rho_0 L\overline{\langle w''q_t''\rangle}$ (long–short-dashed); (c) resolved TKE (solid), SGS TKE (dashed); (d) $\overline{q}_l$ and $\overline{N}$; (e) resolved $\rho_0 L\overline{w'q_l'}$ and $\overline{w'N'}$; and (f) $\overline{r}_e$.

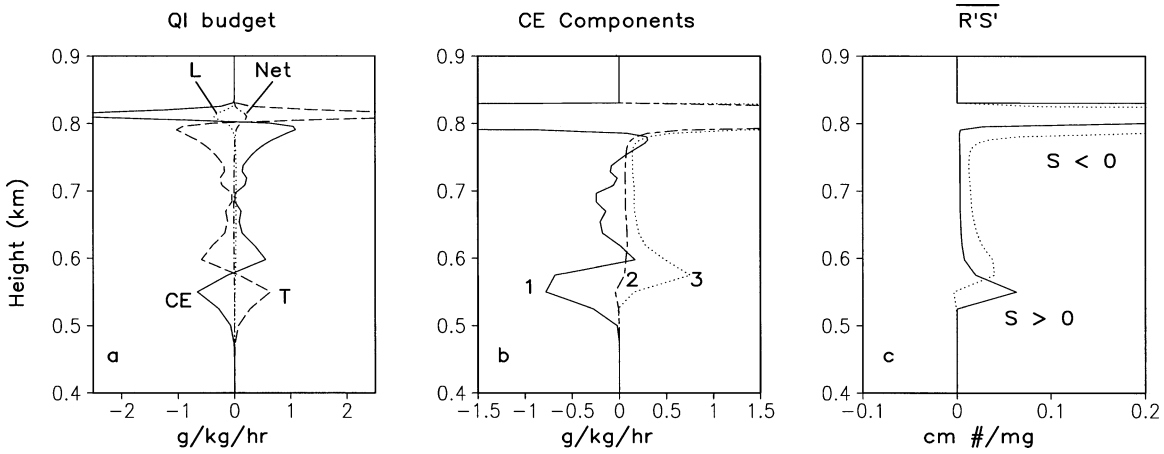

FIG. 2. The $\overline{q}_l$ budget defined by (6). (a) Condensation (CE, solid), the flux divergence (T, dashed), the subsidence (L, dotted), net tendency (Net, dot–dash); (b) $\overline{R}\,\overline{S}$ term (denoted by 1), $\overline{q_l'S'}$ term (denoted by 2), and $\overline{N'S'}$ term (denoted by 3) [the numbers represent corresponding terms in Eq. (6)]; (c) $\overline{R'S'}$ for positive S (solid) and for negative S (dotted).

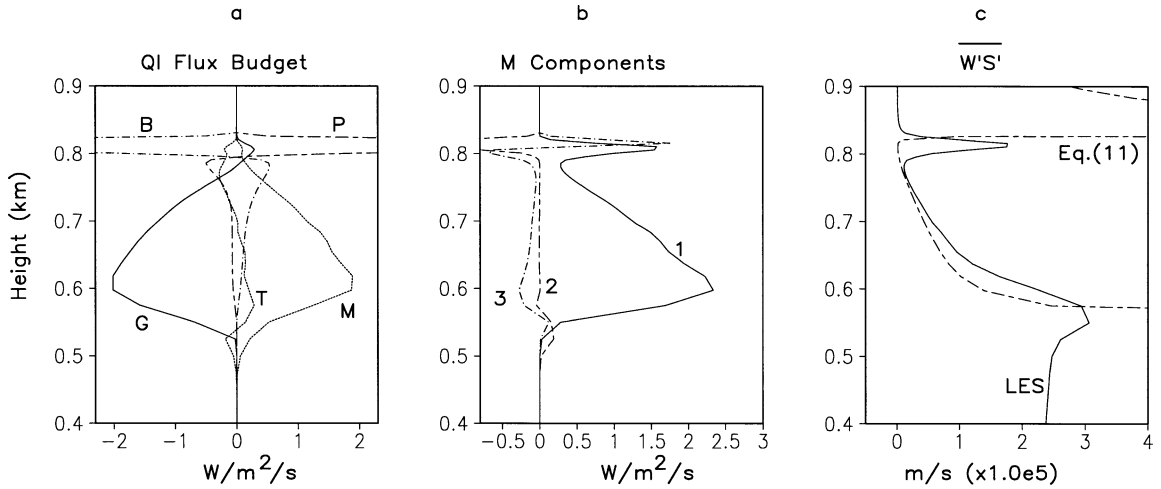

FIG. 3. The $\overline{w'q_l'}$ budget defined by (7). (a) Microphysical term (M representing the square bracket term), mean gradient (G), transport (T), buoyancy correlation (B, dot–dash), and pressure correlation (P, long–short-dashed); (b) $\overline{w'S'}$ term (denoted by 1), ($\overline{w'q_l'}\,\overline{q}_l^{-1} + 2\overline{w'N'}\,\overline{N}^{-1}$) term (denoted by 2), and triple correlation term (denoted by 3) [numbers represent corresponding terms in the square bracket of (7)]; (c) LES-BM resolved $\overline{w'S'}$ (solid) and the approximated by (11) (long–short-dashed). The SGS term is significantly smaller than the other terms and is not shown.

flux (Fig. 1e) are largely a result of turbulent transport of liquid water in the downdrafts. The net condensation is balanced by the flux divergence between 580 and 640 m. In the middle of the cloud layer (700 m), both the flux divergence and CE terms are small, indicating that there are no source and sink terms at those levels. Just below the cloud top (between 720 and 780 m) both the divergence and the net condensation are significantly increased by radiative cooling. Finally, at the cloud top, the turbulent eddies transport the droplets to the warmer and drier inversion where significant evaporation occurs.

Figure 2b shows various terms of the CE term in (6). The mean saturation term is almost always negative from the cloud base up to 750 m except at the level of 600 m where the mean condition is saturated due to considerably supersaturated updrafts. The negative $\overline{S}$ clearly results from considerable subsaturation in the downdrafts despite the water vapor surplus in the updrafts. Near the cloud top ($\sim$780 m), this term is positive because of strong radiative cooling. At cloud top, the warmer and drier air in the inversion leads to large negative values of the mean saturation term.

In contrast to the mean saturation term, contributions from the two turbulence covariance terms are generally positive; a larger S tends to result in more condensation/activation or less evaporation, leading to positive covariance $\overline{N'S'}$ and $\overline{q_l'S'}$. In addition, $\overline{N'S'}$ dominates $\overline{R'S'}$ term due to the activation in updrafts and the evaporative loss in downdrafts near the cloud base.

Recall from (3) that these two turbulence terms represent the correlation between R and S and therefore, $\overline{R'S'} > 0$. Furthermore, Fig. 2c shows that for either positive S or negative S, $R'S'$ is almost always positive. This means that the effects of the turbulence are to enhance the mean CE rate by increasing condensation in the updrafts (usually $S > 0$) as well as decreasing the evaporation in the downdrafts (usually $S < 0$). Therefore, without the turbulence covariance terms, the mean CE rate not only ignores the condensation in the updrafts, but also overestimates the evaporation in the downdrafts. This is particularly true at cloud base and cloud top, as shown in Fig. 2b. This analysis shows that the mean supersaturation should not be used as the *only* factor to drive the droplet growth and the covariance $\overline{R'S'}$ needs to be represented in the CE term. Note that these turbulence terms have been ignored in previous coupled turbulence closure-bin-microphysical models (e.g., Ackerman et al. 1995; Bott et al. 1996).

b. The $\overline{w'q_l'}$ budget

The most striking feature in the $\overline{w'q_l'}$ budget shown in Fig. 3a is a close balance below 700 m between the gradient (G) and the microphysical terms in (7). The mean gradient term represents the traditional downgradient transport (or the diffusive mixing). Its large negative values are a direct result of the large gradient of $\overline{q_l}$ with height, while the positive values of the microphysics term are due to the fact that condensation mainly occurs in the updrafts while evaporation is likely to occur in the downdrafts, leading to a positive correlation between w and CE perturbations. Therefore, it is condensation (evaporation) in the updrafts (downdrafts) that results in positive (negative) q_l fluctuations and leads to a mostly positive liquid water flux for both updrafts and downdrafts.

The buoyancy term is positive below 760 m in the cloud layer where the buoyancy fluctuations are positively correlated with vertical velocity, and it becomes

strongly negative at the cloud top due to the entrainment of more buoyant and drier air. The pressure correlation term is negative below 760 m and becomes strongly positive in the inversion, therefore it tends to cancel the contribution of the buoyancy term. This is consistent with the general description of the corresponding terms in other scalar flux budgets (Moeng 1986).

The first three components of the microphysical part in (7) are presented in Fig. 3b. The fourth is negligibly small due to the small radius ($\sim$1.5 μm) at which droplets are activated, and thus is not included. The contribution of the $\overline{w'S'}$ term dominates the other two from the cloud base up to 770 m, above which it tends to cancel out the negative contribution from the others. The covariance $\overline{w'S'}$ (Fig. 3c) represents a fundamental element of the interaction between the turbulence and microphysics, and thus is essential to the microphysical term. The maximum value just above the cloud base is clearly associated with large positive (negative) S and w in the updrafts (downdrafts) at those levels as discussed by many authors (e.g., Stevens et al. 1996a). At the very top levels of the cloud layer, the warmer and drier inversion air ($S' < 0$) is entrained into the downdrafts ($w' < 0$), leading to the second maximum of the $\overline{w'S'}$ profile.

Recently, Khairoutdinov (2000, personal communication) showed analytically that $\overline{w'S'}$ is the term needed to approximately balance the mean gradient term. To demonstrate this, we consider two major source terms for $\overline{w'S'}$ in the steady-state form of the S tendency equation (e.g., Clark 1973):

$$\frac{dS}{dt} = \left(\frac{\gamma}{L} - \frac{q_s}{R_d T}\right) gw - (1 + \gamma)\frac{dq_l}{dt} = 0$$

$$\Rightarrow \left(\frac{\gamma}{L} - \frac{q_s}{R_d T}\right) gw - (1 + \gamma) 4\pi\rho_l \overline{G} R S = 0, \quad (10)$$

where $\gamma = Lc_p^{-1}\overline{T}\,\overline{\theta}^{-1}\partial q_s/\partial T$ and is considered a known function of the ensemble mean atmospheric pressure and temperature. Assuming R in (10) remains the ensemble mean value, multiplying by w', and performing Reynolds averaging, we have

$$\overline{w'S'} \cong \frac{\overline{w'^2}}{b\overline{R}(1 + \gamma)}\left(\frac{\gamma}{L} - \frac{\overline{q}_s}{R_d\overline{T}}\right) g \cong -\frac{\overline{w'^2}}{b\overline{R}}\frac{d\overline{q}_{sa}}{dz}, \quad (11)$$

where dq_{sa}/dz is the gradient of saturation water vapor mixing ratio following the mean moist adiabat. Note that (11) only applies to the levels where all the grid points are cloudy. Equation (11) states that $\overline{w'S'}$ is always positive, and is equivalent to the correlation between w and the moist adiabatic CE rate ($-wd\overline{q}_{sa}/dz$). The estimated $\overline{w'S'}$ based on (11) is shown in Fig. 3c for comparison. Replacing $\overline{w'S'}$ in (7) with (11) and neglecting SGS and other microphysical terms, leads to

$$\frac{\partial\overline{w'q_l'}}{\partial t} \cong -\overline{w'^2}\frac{\partial\overline{q}_l}{\partial z} - \overline{w'^2}\frac{d\overline{q}_{sa}}{dz} - \frac{\partial\overline{w'w'q_l'}}{\partial z} + \frac{g}{\theta_0}\overline{\theta_v' q_l'} - \frac{1}{\rho_0}\overline{q_l'\frac{\partial p'}{\partial z}}. \quad (12)$$

Therefore, as long as $\overline{q_l}$ follows the mean moist adiabat, which is approximately true for stratocumulus clouds, the mean gradient and $\overline{w'S'}$ terms nearly cancel each other. It is interesting to note that $\overline{w'S'}$ is inversely proportional to $\overline{R}$, which depends on the droplet distribution and the droplet number $\overline{N}$. This point is discussed further in section 7.

This analysis shows that the $\overline{w'S'}$ term balances the negative contribution of the gradient term to produce the positive $\overline{w'q_l'}$. Therefore, this term must be considered in the parameterization of $\overline{w'q_l'}$ when a bin-microphysical model is coupled to a turbulence parameterization.

c. The N budget

As in the case of the $\overline{q_l}$ budget, the flux divergence (T) and microphysical terms ($A + E$) in (8) are closely balanced in the $\overline{N}$ budget (Fig. 4a). Particularly, both terms have large magnitudes in the lower part of the cloud layer, implying significant activation/evaporation and turbulent transport of the droplets there. At the cloud top, both terms reach their local maximum although the magnitudes are significantly lower than those at the cloud base.

Figure 4b shows the activation (A) and the evaporation (E) components in the microphysical term. Below cloud base, the evaporation is likely to have resulted from the downward transport of small cloud droplets, which leads to the $\overline{w'N'}$ convergence. Both the activation rate and the flux divergence reach a maximum at 575 m, implying that the newly activated cloud droplets at the cloud base are effectively transported upward to the upper levels of the cloud layer. At the cloud top, both activation and the evaporative loss attain second local maxima, which may be strongly influenced by the spurious production of cloud drops due to the LES-BM inability to represent SGS cloud field at cloud edges as discussed by Stevens et al. (1996b). The droplets are generally larger at the cloud top than those at the cloud base (in the absence of drizzle processes), leading to a reduced loss of the droplets due to evaporation at cloud top compared with that at cloud base.

d. The $\overline{w'N'}$ budget

As shown in Fig. 5a, the gradient and the microphysical terms again have opposite signs and are dominant in the budget in the lower part of the cloud. In the inversion layer, the buoyancy and pressure perturbation terms are in close balance. Figure 5b shows that both components of the microphysical term, the acti-

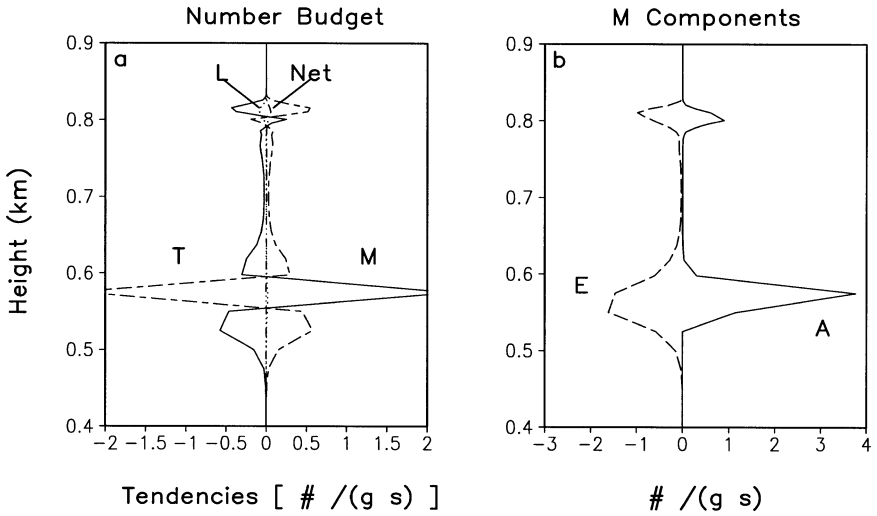

FIG. 4. The $\overline{N}$ budget defined by (8). (a) The flux divergence (T, long–short-dashed), microphysics [$M = A + E$ in Eq. (8), solid], subsidence (L, dotted), and net tendency (dot–dash); (b) activation (A) and evaporation (E).

vation and evaporation fluxes as defined by "A" and "E" terms in (9), are generally positive, because the activation is most likely to occur in the updrafts and the evaporation in the downdrafts. Similar to the budget of $\overline{w'q_l'}$, the results here indicate that $\overline{w'N'}$ should not be modeled as a diffusive flux, because the activation and the evaporation contribute significantly and positively to the flux. Without these positive contributions, $\overline{w'N'}$ would be largely negative and not be able to transport the newly activated droplets at the cloud base to upper levels to maintain a uniform profile of $\overline{N}$ in the middle of the cloud layer.

6. Parameterizations

The above results clearly demonstrate the importance of turbulence–microphysics interaction in defining the ensemble mean CE rate and various liquid water–related fluxes. Therefore, any attempt to parameterize these variables must include both turbulence and microphysical statistics.

a. Liquid water flux $\overline{w'q_l'}$

Two types of parameterizations have been frequently used for the stratocumulus cloud parameterizations. The first, and the most popular one, is the statistical approach of Sommeria and Deardorff (1977) and Mellor (1977); (or some variation thereof) and can be written as

$$\overline{w'q_l'} = \frac{C \cdot \left(\overline{w'q_t'} - \dfrac{c_p\gamma}{L}\overline{w'\theta_l'}\right)}{(1 + \gamma)}, \qquad (13)$$

where C is cloud fraction, q_t total water mixing ratio, and θ_l liquid water potential temperature. Note that (13) is not related to the cloud droplet spectrum because liquid water is diagnosed by any excess above the saturation mixing ratio (saturation adjustment scheme); that is, $S = 0$ at any cloudy grid point. Wang and Wang (1999) analyzed (13) and concluded that the turbulence-generated condensation is dominant in defining the flux profile in the parameterization. The second parameterization is the mass flux scheme in which $\overline{w'q_l'}$ is parameterized as a product of a mass flux and the difference between updraft and downdraft liquid water content. Wang and Albrecht (1986) used this method to compute the buoyancy flux in their modified mixed layer model. Randall (1987) discussed this approach in detail; it can be expressed in general as

$$\overline{w'\varphi'} = \sigma_u w_u(\varphi_u - \varphi_d), \qquad (14)$$

where subscripts "u" and "d" represent updraft and downdraft variables, σ is the fractional coverage of either updrafts or downdrafts, w_u the average updraft velocity, and φ any variable ($\varphi = q_l$ for liquid water flux), respectively.

Based on the $\overline{w'q_l'}$ budget analysis presented in section 5b, a new dynamic and microphysical approach is proposed here. Following the common practice of second-order flux parameterization, the tendency of (7) is set to zero for the equilibrium solution to $\overline{w'q_l'}$. In addition, the pressure correlation term is split into a buoyancy and a return-to-isotropy term (e.g., Moeng and Wyngaard 1986); that is, $-1/\rho_0 \times \overline{q_l'\partial p'/\partial z} = -0.5g/\theta_0 \times \overline{\theta_v'q_l'} - \overline{w'q_l'}/\tau_R$, where τ_R is return-to-isotropy timescale. Furthermore, the transport term and all the third moments in the microphysical term are neglected. The two second-order turbulence–microphysics covariance terms of (7) are assumed to be related by

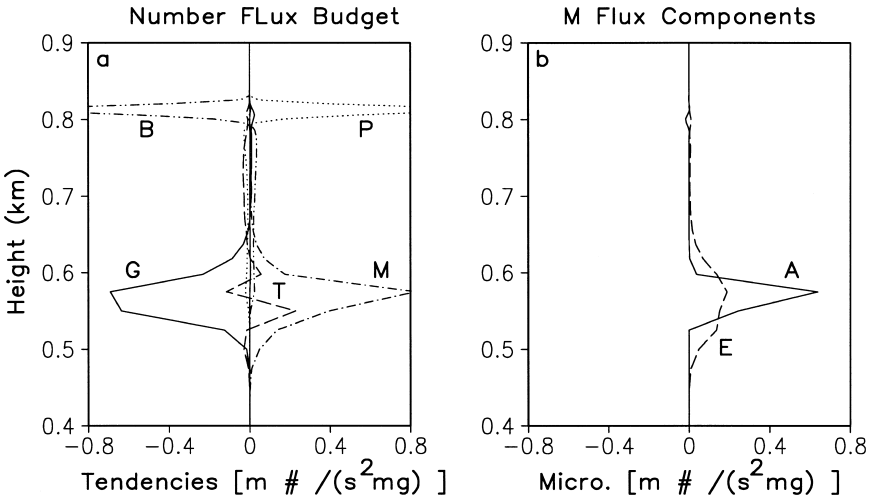

FIG. 5. The $\overline{w'N'}$ budget defined by (9). (a) Activation/evaporation flux terms ($M = A + E$ in Eq. (9), dot–dash), mean gradient (G, solid), transport (T, dashed), buoyancy correlation (B, dot–dot–dash), pressure correlation (P, dotted); (b) activation flux term (A, solid), evaporation flux term (E, dashed). The SGS term is significantly smaller than the other terms and is not shown.

$$\overline{w'q_l'}/\overline{q}_l \approx \overline{w'N'}/\overline{N}. \tag{15}$$

Using the definition of $q_t (q_t = q_v + q_l)$ and S, we have $S' = q_t' - q_l' - q_s'$ (T, p). Further expressing q_s' in terms of θ_l' and q_l', we can approximate S' as

$$S' \cong q_t' - \frac{c_p\gamma}{L}\theta_l' - (1 + \gamma)q_l', \tag{16}$$

where the effects of pressure fluctuations are neglected. An expression of $\overline{w'S'}$ can be derived from (16), and is then substituted into (7) to obtain

$$\overline{w'q_l'} = \frac{\tau_R\left(-\overline{w'^2}\frac{\partial\overline{q}_l}{\partial z} + 0.5\frac{g}{\theta_0}\overline{\theta_v'q_l'}\right) + \frac{\tau_R}{\tau_{\rm CE}(1+\gamma)}\left(\overline{w'q_t'} - \frac{c_p\gamma}{L}\overline{w'\theta_l'}\right)}{1 + \frac{\tau_R}{\tau_{\rm CE}}\left(1 - \frac{\overline{S}}{\overline{q}_l(1+\gamma)}\right)}, \tag{17}$$

where τ_R is of the same order as the large eddy turnover time (Moeng and Wyngaard, 1986), and $\tau_{\rm CE}$ is the CE timescale defined by

$$\tau_{\rm CE} = \frac{1}{4\pi\rho_l(1+\gamma)\overline{G}\,\overline{R}}. \tag{18}$$

Note that $\tau_{\rm CE}$ is the same as the commonly used supersaturation absorption or phase relaxation timescale defined by an e-folding decrease of the initial surplus water vapor discussed by many authors (e.g., Squires 1952; Kogan et al. 1995).

Parameterization (17) represents a balance among three dynamic and one microphysical terms in (7); these terms are the mean gradient, buoyancy, pressure correlation, and surplus vapor flux terms. An interesting feature of (17) is that $\overline{w'q_l'}$ is directly related to $\tau_{\rm CE}$, which is defined by the droplet spectrum through (18). A smaller $\tau_{\rm CE}$ (or larger $\overline{R}$) would tend to reduce the effect of the mean gradient term, which can be explained as follows. The *effective* timescale over which the turbulence can affect $\overline{w'q_l'}$ is $(1/\tau_R + 1/\tau_{\rm CE})^{-1}$ (rather than τ_R), as shown by (17). Therefore, when $\tau_R/\tau_{\rm CE} \gg 1$, the turbulence has a response timescale that is equivalent to $\tau_{\rm CE}$ to counteract the microphysical change. Consequently, a smaller $\tau_{\rm CE}$ would result in a smaller turbulence diffusion flux and a larger $\overline{w'q_l'}$. Considering both the turbulence and condensation timescales, we would have two limiting cases. If $\tau_R/\tau_{\rm CE} \to 0$, $\overline{w'q_l'}$ can be represented by the turbulence part only, which is simply the traditional downgradient formulation. If $\tau_R/\tau_{\rm CE} \to \infty$, $\overline{w'q_l'}$ is determined by the microphysical part only, which is similar to (13). These two formulations represent only two extreme cases in which either turbulence or microphysical contributions dominate.

For real clouds, both τ_R and $\tau_{\rm CE}$ are finite. For example, given the generalized convective velocity scale

(Deardorff 1980) $w_* \cong 0.9$ m s^{-1} and the boundary layer height $z_i \cong 800$ m, we obtain $\tau_R \sim z_i/w_* \cong 880$ s. Figure 6a shows that τ_{CE} is between 3 and 10 s. Clearly, $\tau_{CE} \ll \tau_R$, demonstrating that the microphysical processes are always important and cannot be ignored. Since the gradient of $\overline{q}_l$ is significant for stratocumulus clouds, the turbulence diffusion term is large and must also be included for a supersaturation-based cloud model as well.

Assuming the equilibrium condition in (12), using the same parameterization for the pressure correlation term and ignoring the resultant buoyancy term, we obtain the following approximation:

$$\overline{w'q_l'} \cong -\tau_R \overline{w'^2}\left(\frac{d\overline{q}_{sa}}{dz} + \frac{\partial \overline{q}_l}{\partial z}\right). \tag{19}$$

This equation states that $\overline{w'q_l'}$ can be treated as a downgradient flux, as long as the fluctuation of q_l resulting from vertical motion includes both the condensation/evaporation and the gradient parts. However, a major weakness of (19) is that the microphysical contribution is independent of τ_{CE} due to the approximations made in deriving (11). Consequently, both the turbulence and CE contributions depend *only* on the turbulence timescale τ_R. [See Eq. (17) for comparison.] Note that (19) has been obtained by Khvorostyanov and Curry (1999) and Sigg (2000). The development in this paper differs from theirs mainly in that (17) and (19) are derived from the dynamic balance among the turbulence and microphysical processes.

Figures 6b and 6c show the comparison between the LES-BM resolved and the parameterized fluxes. The parameterized $\overline{w'q_l'}$ from (17) compares well with the LES-BM resolved flux except in the inversion where the negative values result, probably from the buoyancy term. For this reason, $\overline{w'q_l'}$ is again calculated from (17) but without the buoyancy term. The new flux performs better in the inversion. The parameterized $\overline{w'q_l'}$ from (13) and (14) are also shown (Fig. 6c). Because the mass flux scheme (14) ignores the variability *within* updraft or downdraft plumes, it understandably underestimates $\overline{w'q_l'}$. The statistical approach is based on a Gaussian distribution of the moisture departure from the mean saturation, and based on the saturation adjustment practice. Therefore, if $C = 1$ at certain levels (i.e., all the grid points are cloudy at that level), the value calculated from (13) should be almost equal to the LES resolved flux if the saturation adjustment were used in the model. The flux from (13) is, however, significantly larger than the LES-BM resolved flux. This implies that an LES coupled with a saturation adjustment (SA) cloud scheme gives larger $\overline{w'q_l'}$ than an LES coupled with a supersaturation-based cloud model. This result will be discussed further in section 7.

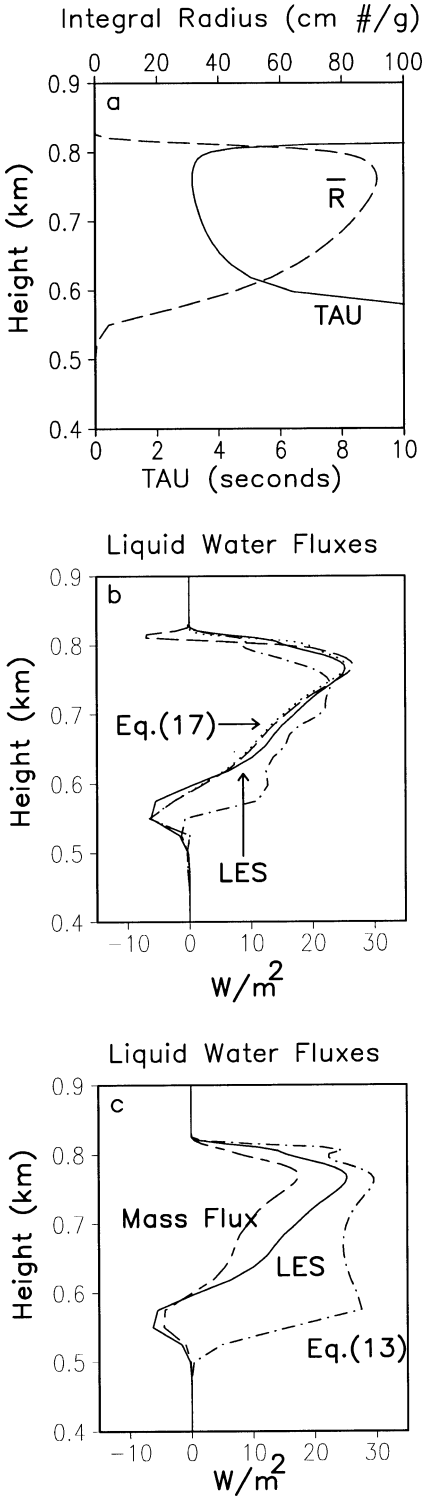

FIG. 6. The $\overline{w'q_l'}$ parameterization. (a) Integral radius ($\overline{R}$, dashed) and the CE timescale (TAU, solid) defined by (18); (b) the LES-resolved $\overline{w'q_l'}$ (LES, solid), parameterization (17) with B term (long-dashed), parameterization by (17) *without* B term (dotted) and the calculated from (15) (dot–dash); (c) $\overline{w'q_l'}$ by the mass flux parameterization (14) (long–short) and LES-resolved (solid), $\overline{w'q_l'}$ by (13) (dot-dash).

b. Droplet number density flux $\overline{w'N'}$

Using the equilibrium and return-to-isotropy assumptions, we can obtain the following diagnostic equation from (9):

$$\overline{w'N'} = \tau_R\left(-\frac{\partial\overline{w'w'N'}}{\partial z} - \overline{w'^2}\frac{\partial\overline{N}}{\partial z} + 0.5\frac{g}{\theta_0}\overline{\theta_v' N'} + \overline{w'A_N'} + \overline{w'E_N'}\right), \quad (20)$$

where the transport term is included because it is important in the middle of the cloud layer as shown in Fig. 5. The mass flux formulation for $\overline{w'N'}$ can be obtained by letting $\varphi = N$ in (14). As shown in Fig. 7, the flux without the transport term derived from (20) does not even provide solutions of reasonable magnitude. However, the inclusion of the transport term significantly improves the parameterization, although its performance is still less satisfactory than (17) for $\overline{w'q_l'}$. The main reason lies in the fact that all the terms are small and of the same order as that of the tendency term in the middle cloud layer. The simple relationship (15) compares well with the resolved $\overline{w'N'}$ at the cloud base and in the upper part of the cloud layer. However, it does not obtain the maximum above the cloud base because the activation contributes little to $\overline{w'q_l'}$ as discussed in the budget analysis. In contrast, the mass flux formulation (14) obtains the correct positive maximum because the activation and evaporation contribution is automatically included in N_u and N_d, respectively, while it considerably underestimates the negative values near the cloud base.

Although the parameterizations of $\overline{w'q_l'}$ and $\overline{w'N'}$ are derived for the ensemble mean fluxes, some of them may also be used for the SGS fluxes in LES-based microphysical parameterizations like those of Feingold et al. (1998) and Khairoutdinov and Kogan (2000). Normally, the SGS cloud water mass and number fluxes are parameterized in terms of the diffusion formulation as those of q_t and θ_l. However, the major difference between q_l and q_t is that the former typically increases significantly with height due to condensation, while the latter is conserved during condensation and is therefore usually well mixed in the boundary layers. For an LES, the subgrid-scale diffusion timescale τ_R can be estimated as Δz (SGS TKE)$^{-0.5} \sim 100$ s using the simulation parameters, and is still significantly larger than $\tau_{\rm CE}$. Therefore, the microphysical impact should be considered in formulating the SGS liquid water fluxes.

c. Ensemble mean CE rate

At the heart of any microphysical parameterization is the mean CE rate, which must include the turbulence contribution as discussed in the last section. One possibility is to use a higher-order turbulence closure model

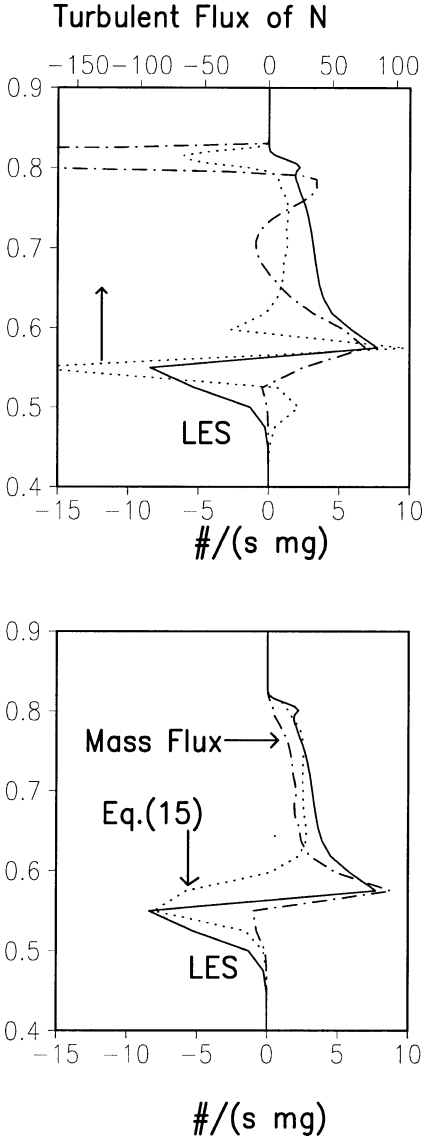

FIG. 7. The $\overline{w'N'}$ parameterization. (top) LES-resolved flux (solid, bottom axis), Eq. (20) *without* the transport (dotted, top axis); Eq. (20) *with* the transport (dot–dash, bottom axis). (bottom) LES-resolved flux (solid), the mass flux parameterization (14) (dot–dash), Eq. (15) (dotted).

to directly predict or diagnose $\overline{q_l'S'}$ and $\overline{N'S'}$ in (6). This can be accomplished by deriving the budgets of $\overline{q_l'S'}$ and $\overline{N'S'}$ following the approach of Wang et al. (1998) and Wang and Wang, (2000).

Another approach is to recognize that the turbulent updraft and downdraft circulation is responsible for most of the turbulent transport and that vertical motion is the main driving force for the microphysics. Therefore, we could compute CE rates in each of the updraft and downdraft branches; that is, we could rewrite (3) as

$$\left(\frac{\partial\overline{q_l}}{\partial t}\right)_{\rm CE} \cong 4\pi G(\overline{T}, \overline{p})\rho_l(\sigma_u R_u S_u + \sigma_d R_d S_d). \quad (21)$$

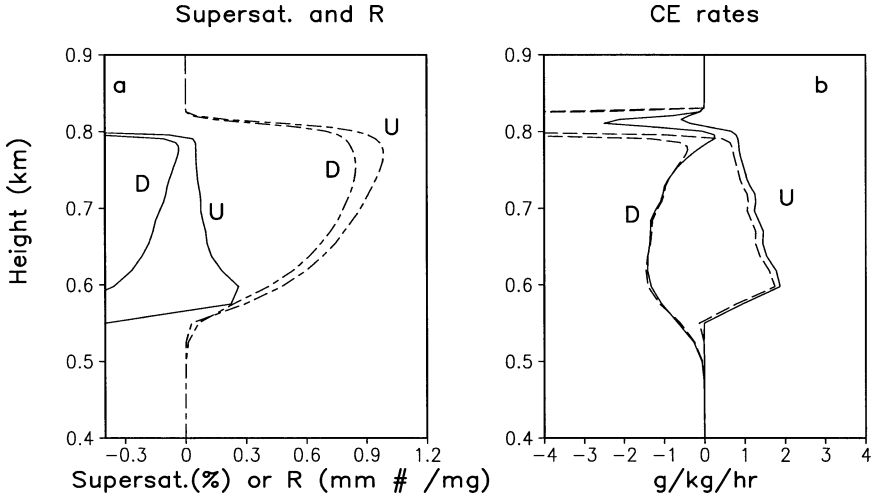

FIG. 8. The CE parameterization defined by (21). (a) Average supersaturation for updrafts (U, solid) and downdrafts (D, solid), integral radius for updrafts (U, dashed) and downdrafts (D, dashed). (b) Updraft CE rate from the LES (U, solid) and parameterization (21) (U, dashed), downdraft CE rates from the LES (D, solid) and parameterization (21) (D, dashed).

The supersaturation and the integral radius of updrafts and downdrafts demonstrate normal profiles as shown in Fig. 8 (and derived from S1). Profiles of the parameterized updraft and downdraft CE rates closely follow those from direct conditional sampling of LES-BM model resolved CE rates in most of the cloud layer. This consistency reflects the coherence between w and S at those levels, which is the basis for the parameterization. The consistency does not, however, exist in the inversion layer because the circulation is ill-defined there due to strong influences of small-scale turbulence. Therefore, even though (21) can accurately describe the CE process in most of the cloud layer, a special treatment of the entrainment zone at the cloud top must be formulated to include the effects of small-scale turbulence. A similar framework was used by Considine (1997) to study diurnal variability in microphysical properties of stratocumulus clouds. Note that (21) has the same form as the mass flux representation of the turbulence statistics in many models (e.g., Wang and Albrecht 1986; Lappen and Randall 2001). Therefore, it may be particularly useful in a coupled mass flux–microphysics parameterization.

7. Discussion

a. Dynamic feedback of the CE timescale

The results in section 6a (Fig. 6) suggest that $\overline{w'q_l'}$ resolved by an LES coupled with a saturation adjustment cloud scheme is larger than that resolved by a LES coupled with a supersaturation-based cloud model. The reason lies with the fact that $S = 0$ at a cloudy grid point for a LES-SA, while it can be greater or smaller than zero at a cloudy grid for a LES-BM. This can be expressed in the following relationship obtained from (16):

$$\overline{w'q_l'} = \frac{1}{1 + \gamma}\left(\overline{w'q_t'} - \frac{c_p\gamma}{L}\overline{w'\theta_l'} - \overline{w'S'}\right), \quad (22)$$

where $\overline{w'S'}$, while always positive for the LES-BM model, is zero for the LES-SA at a level at which all the grid points are cloudy. Equation (22) shows that $\overline{w'q_l'}$ derived from LES-SA is larger than that from LES-BM when all the grids are cloudy. In other words, LES-SA produces more condensation in updrafts and evaporation in downdrafts than LES-BM does because S must be zero for a saturation adjustment when cloud is present. Consequently, the magnitudes of q_l' and w' from LES-SA are larger than those from LES-BM.

The above results suggest that the CE timescale τ_{CE}, to some extent, regulates the turbulence field. Note that droplet number N is related to τ_{CE} through the integral radius R. When N is large, R is large, leading to a small τ_{CE} as seen from (18). Then, larger CE fluctuations are produced and result in larger $\overline{w'q_l'}$. Therefore, the larger N is, the smaller τ_{CE} is, and the closer the turbulence structure derived from LES-BM is to that derived from LES-SA. More specifically, when τ_{CE} decreases (i.e., R increases), $\overline{w'S'}$ decreases as shown by (11), resulting in an enhanced $\overline{w'q_l'}$ as shown by (22). This feedback can also be seen from the $\overline{w'q_l'}$ parameterization (17). Since the negative contribution from the gradient term decreases with decreasing τ_{CE}, $\overline{w'q_l'}$ increases with increasing N and approaches (13) when $\tau_{CE} \to 0$. Because the extra q_l' produced by larger N (or smaller τ_{CE}) in up- and downdrafts are likely to cancel for the ensemble mean due to their different signs, and because instantaneous CE rate is strongly coupled to the vertical mo-

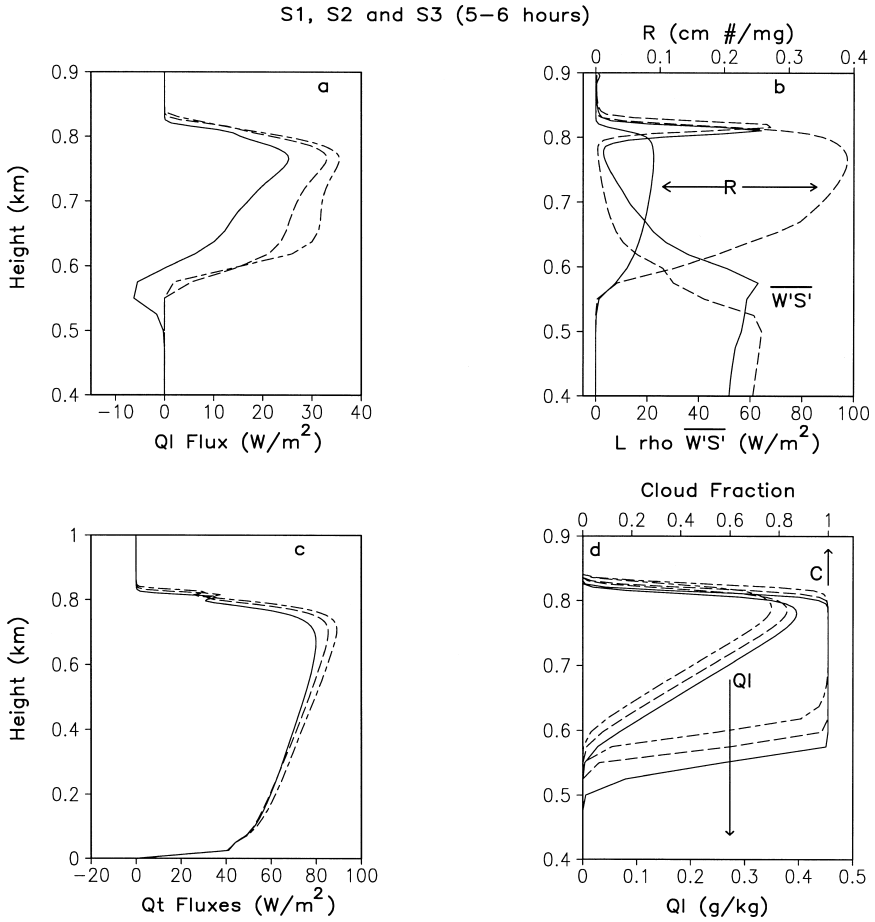

FIG. 9. Impacts of N and the saturation adjustment. (a) Resolved $\rho_0 L\overline{w'q_l'}$; (b) integral radius (R) and $\rho_0 L\overline{w'S'}$; (c) $\rho_0 L\overline{w'q_t'}$; (d) $\overline{q}_l$ and cloud fraction (C). Solid lines denote S1, long-dashed S2, and long–short-dashed S3.

tion of turbulent eddies, the direct impact of this feedback is on the turbulence field.

To test these ideas, two more simulations are performed. One (S2) uses the same LES-BM model, but with a background CCN number of 1000 mg^{-1}. The other (S3) uses the same LES dynamic model but with a saturation adjustment scheme. The high CCN number concentration used in S2 is chosen to facilitate discussion, but it may not be unrealistic for a polluted air mass. All the simulation procedures are identical to those of the previous simulation (S1) and listed in Table 1.

Figure 9 shows the comparison of some statistics among three simulations over the last hour (hour 5–6). Both S2 and S3 result in significantly larger resolved $\overline{w'q_l'}$ than S1, as expected from the above discussion. Particularly, $\overline{w'q_l'}$ from S2 is closer to S3 than to S1, despite the fact that S3 is run with the LES-SA model, while S1 and S2 are run with the LES-BM. The integral droplet radius $\overline{R}$ in S2 is about four times that of S1, leading to a reduction in $\overline{w'S'}$ from S2. This result is consistent with the earlier discussion in which we argued that an increase in $\overline{R}$ will decrease $\overline{w'S'}$ and thus increase $\overline{w'q_l'}$. Since local CE rates in turbulent eddies increase with $\overline{R}$ (or decreasing τ_{CE}), the cloud-top entrainment is enhanced, which is demonstrated by the larger total water flux near the cloud top, and consequently $\overline{q}_l$ and cloud fraction from S3 are reduced as shown in Fig. 9d. Because LES-SA results in the largest instantaneous local CE rate among the three simulations, the entrainment from S3 is strongest and $\overline{q}_l$ is the smallest, as can be seen in both Figs. 9c and 9d.

The above results suggest that different CCN number concentrations may lead to different turbulence fields due to the different CE timescales. Consequently, the impact of variable CCN number density is not only due to the drizzle process, but also due to the different CE timescale.

b. Impact of drizzle on the parameterizations

The parameterizations (17) and (20) have been derived based on the formulation without drizzle processes. It is natural to ask how drizzle will affect these parameterizations. To answer this question, we perform

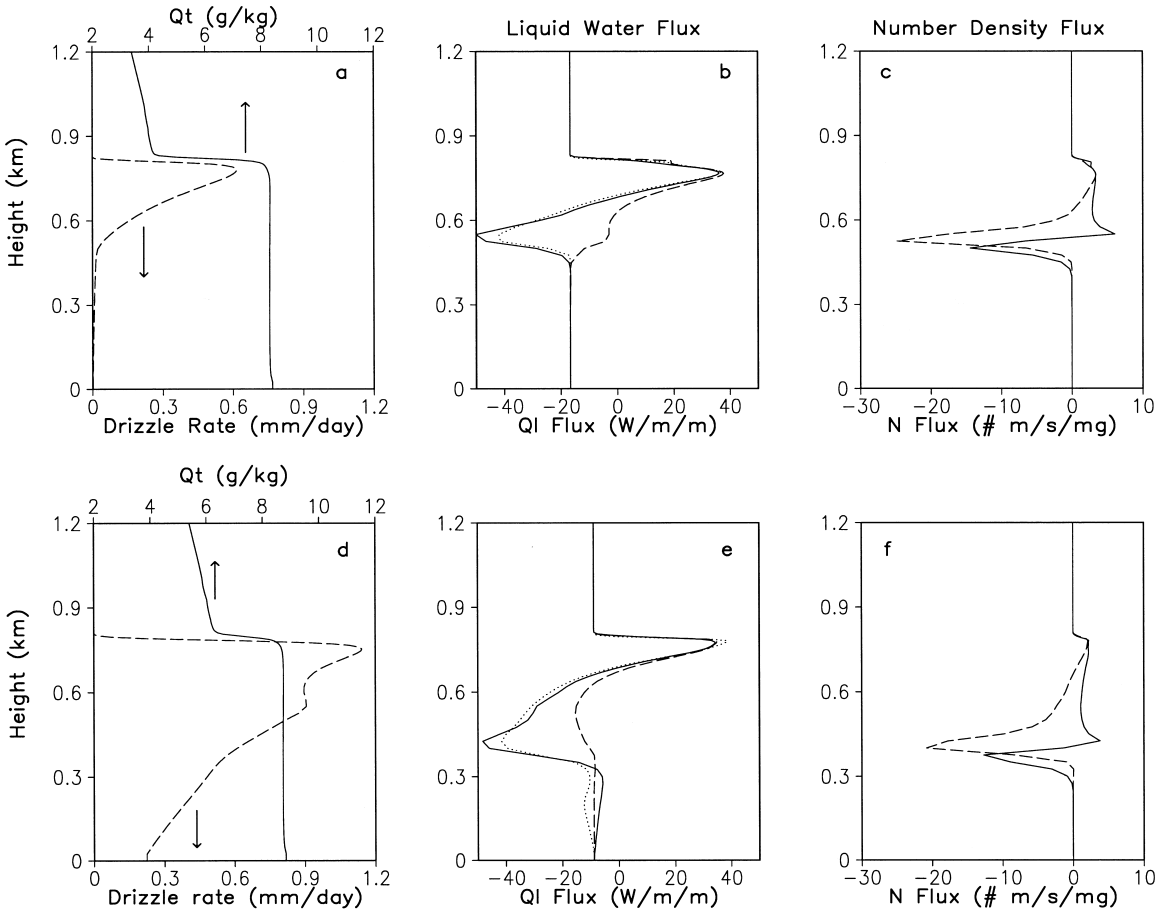

FIG. 10. Impact of drizzle on the parameterizations. (top) Simulation S4, (bottom) S5. (left) Drizzle rate (dashed) and $\overline{q}_t$ (solid); (center) $\rho_0 L\overline{w'q_l'}$, LES-resolved (solid), parameterization (17) (dotted), Eq. (13) (dashed); (right) $\overline{w'N'}$, LES-resolved (solid), Eq. (15) (dashed).

two simulations (S4 and S5) that include the processes of droplet coalescence–collection and sedimentation as shown in Table 1. In S5, the higher water vapor mixing ratio above the cloud leads to a stronger drizzle rate as seen in Fig. 10a. The flux $\overline{w'q_l'}$, calculated from parameterization (17) without the buoyancy term compares well with the LES-BM solution. This is because the drizzle contribution to the $\overline{w'q_l'}$ budget is at least one order of magnitude smaller than the major terms (not shown here), and thus can be neglected. Therefore, (17) should apply as long as the dynamics are primarily driven by the cloud-top radiative cooling (rather than by convective instability in the shallow cumulus regime). The fluxes based on the saturation adjustment scheme (13) considerably overestimates the flux value in the lower half of the cloud layer where τ_{CE} is relatively large (Fig. 6a) and S has a positive maximum value in updrafts.

The inclusion of drizzle may affect parameterization (20) through the correlation between w' and droplet collection, and sedimentation, respectively. We have found in particular that the contribution from the collection tendency flux is significant and highly variable, and thus the quasi-equilibrium condition is not met for the $\overline{w'N'}$ budget. Consequently, the validity of (20) is degraded. The flux calculated from (15) is compared with the LES-BM resolved in Figs. 10c and 10f, and the discrepancies are relatively large compared to those for $\overline{w'q_l'}$. Therefore, the formulations (15) and (20) do not provided satisfactory solutions to the $\overline{w'N'}$ parameterization, although they are probably useful steps toward that goal.

The mass flux representation of $\overline{w'q_l'}$, $\overline{w'N'}$, and the ensemble CE rate should not be significantly influenced by the drizzle processes, because the formulations, (14) and (21), only involve the conditional sampling of updraft–downdraft properties. They should apply in drizzle conditions so long as the convective circulation remains the major turbulent transport mechanism.

8. Summary and conclusions

The main objectives of this work are to understand how turbulence interacts with microphysics to produce an ensemble mean CE rate and liquid water fluxes, and to suggest methods to parameterize them. The approach

is to simulate a case of a nonprecipitating stratocumulus cloud with a coupled large eddy simulation and an explicit bin-microphysical model, and then perform a budget analysis for four liquid water variables: $\overline{q_l}$, $\overline{w'q_l'}$, $\overline{N}$, and $\overline{w'N'}$. The major results can be summarized as follows.

The ensemble mean CE rate can be decomposed into mean saturation and turbulence parts; the former is directly computed from the ensemble mean supersatura tion and the latter comes from the covariance $\overline{R'S'}$. The turbulence contribution increases the mean CE rate by enhancing condensation in supersaturated regions ($S > 0$) and reducing evaporation in subsaturated regions ($S < 0$). The dominant component of the turbulence contribution is the covariance $\overline{N'S'}$.

For the liquid water flux budget, a close balance is reached between the negative mean gradient term and the positive $\overline{w'S'}$. Therefore, it is $\overline{w'S'}$ that balances the downgradient diffusive flux to produce a positive $\overline{w'q_l'}$ for the stratocumulus cloud. Based on this result, a new parameterization of $\overline{w'q_l'}$ (17) is proposed for coupled turbulence–microphysical model. The parameterization includes four elements: the downgradient transport, microphysical contribution, turbulent mixing timescale, and condensation timescale. The new parameterization compares favorably with the LES-BM resolved flux for both the drizzle and nondrizzle simulations. The mass flux formulation not only provides reasonable values for $\overline{w'q_l'}$ and $\overline{w'N'}$, but also performs well for the ensemble mean CE rate.

It is shown that the CE timescale defined by (18) may regulate the turbulence dynamics, because a smaller CE timescale tends to result in larger condensation fluctuations, which enhance $\overline{w'q_l'}$. Of particular importance is the approximation (11), which directly relates the turbulence–microphysics forcing $\overline{w'S'}$ to the CE timescale. Consequently, the smaller the timescale is, the larger the flux $\overline{w'q_l'}$ is, as demonstrated by (11) and (22), or (17). Therefore, the droplet number concentration N may affect the turbulence dynamics through the CE timescale. The simulations show that the larger N is, the stronger the entrainment, and the smaller the mean liquid water content. Since an LES-SA *instantly* condenses (evaporates) all available water vapor (liquid water) surplus, it produces stronger entrainment rates and smaller liquid water contents than an LES-BM for nonprecipitating stratocumulus clouds.

Two possible methods of computing the ensemble mean CE rate are proposed. One is to derive budgets for $\overline{q_l'S'}$ and $\overline{N'S'}$ using a higher-order turbulence closure technique, and then predict or diagnose these statistical variables. The disadvantage is that the microphysical source terms in these budgets must be parameterized. The other is to use the mass flux method to compute CE rates for updraft and downdrafts. Although the comparison between this approach and the LES-BM model-resolved CE rates is encouraging, one has to parameterize vertical velocities and thermodynamic variables for each of the branches in a turbulence parameterization. The mass flux boundary layer parameterization developed by Lappen and Randall (2001) could be used to provide these variables. Another possibility is to use various variance and covariance functions with assumed joint probability density functions to compute these updraft and downdraft variables, as suggested by Wyngaard and Moeng (1992).

Understanding the interaction between the turbulence and microphysics is crucial for a successful representation of cloud droplet spectrum in a boundary layer parameterization. This paper shows that parameterization of the condensation, turbulent fluxes of the cloud water mass, and the droplet number concentration should include both the turbulence statistics and cloud droplet spectrum information. The parameterizations developed in this paper are steps towards that goal. One interesting aspect of turbulence–microphysics coupling discussed in the paper is the dynamic feedback of the CE timescale on the coupled turbulence–microphysics field. Immediate questions are as follows. How much does this feedback contribute to the overall impact of changing the CCN number concentration? And how should one represent it in a coupled turbulence–microphysical parameterization? These issues should be addressed in order to fully understand the interaction between the microphysics and turbulence dynamics.

Acknowledgments. We thank Marat Khairoutdinov for the stimulating discussion that lead to Eq. (11) and Bjorn Stevens for providing his LES code. Bjorn Stevens, Charlie Cohen, and Steve Burk are thanked for their comments on the manuscript. The constructive comments of the anonymous reviewers are greatly appreciated. This work was started when S. Wang was affiliated with Universities Space Research Association and supported by the NASA FIRE III and EOS programs. Most of the analyses and writing were done when S. Wang was at Naval Research Laboratory, and supported by the Office of Naval Research under PE 0602435N. Q. Wang was supported by NSF Grants ATM-9700845 and ATM-9900496. G. Feingold acknowledges support from the NSF/NOAA EPIC program.

APPENDIX A

Components of the Ensemble Mean CE Rate

Applying Reynolds averaging operation on (2) gives following ensemble mean equation:

$$\left(\frac{\partial \overline{q_l}}{\partial t}\right)_{\mathrm{CE}} = 4\pi\rho_l(\underbrace{\overline{R}\,\overline{S}\,\overline{G}}_{1} + \underbrace{\overline{G}\,\overline{R'S'}}_{2} + \underbrace{\overline{S}\,\overline{R'G'}}_{3} + \underbrace{\overline{R}\,\overline{S'G'}}_{4} + \underbrace{\overline{G'R'S'}}_{5}), \tag{A1}$$

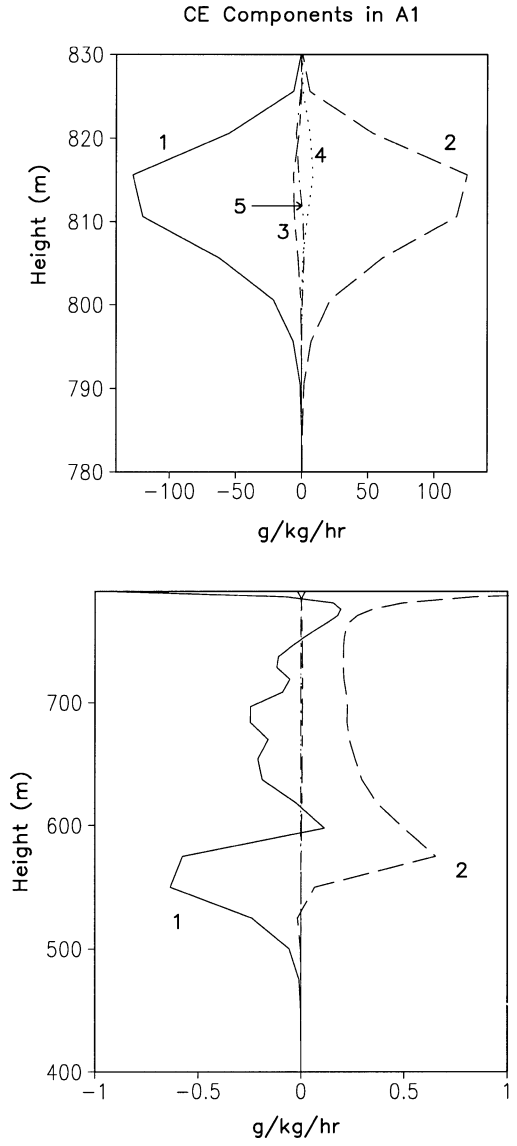

FIG. A1. Comparison among various terms in Eq. (A1): (top) 780 m $\leq z \leq$ 830 m; (bottom) 400 $\leq z \leq$ 780 m. They are $\overline{RSG}$ (line 1, solid), $\overline{GR'S'}$ (line 2, dashed), $\overline{SR'G'}$ (line 3, long–short), $\overline{RS'G'}$ (line 4, dotted), and $\overline{G'R'S'}$ (line 5, dot–dash). The line numbers denote corresponding terms in Eq. (A1). Note, in the lower panel, the values for terms 3–5 are less than 10^{-2} (g kg^{-1} s^{-1}), and thus the lines for these terms cannot be differentiated.

where the numbers under the equation represent corresponding terms. For S1 (see Table 1), profiles of these terms are shown in Fig. A1. The terms 1 and 2 are by far the most dominant in the entire cloud layer. The weak correlation between G and the other variables results from relatively weak dependence of G on temperature. Therefore, it is justified to neglect the last three terms in Eq. (A1) to obtain (2), which is used in the budget analysis.

APPENDIX B

Derivation of Liquid Water Flux Budget

We first subtract (3) from (2), and then include the activation term to obtain the total microphysics fluctuation tendency

$$\left(\frac{\partial q_l'}{\partial t}\right)_{\text{Mic}} = 4\pi\overline{G}\rho_l(\overline{R}S' + \overline{S}R' + R'S' - \overline{R'S'}) + A_c'. \tag{B1}$$

Multiplying by w' on both sides and applying Reynolds averaging operation,

$$\overline{w'\left(\frac{\partial q_l'}{\partial t}\right)_{\text{Mic}}} = 4\pi\overline{G}\rho_l(\overline{R}\,\overline{w'S'} + \overline{S}\,\overline{w'R'} + \overline{w'R'S'}) + \overline{w'A_c'}. \tag{B2}$$

Substituting R' from (5), the above equation becomes

$$\left(\frac{\partial\overline{w'q_l'}}{\partial t}\right)_{\text{Mic}} = 4\pi\overline{G}\rho_l\left[\overline{R}\,\overline{w'S'} + \frac{\overline{R}\,\overline{S}}{3}\left(\frac{\overline{w'q_l'}}{\overline{q}_l} + \frac{2\overline{w'N'}}{\overline{N}}\right) + \frac{\overline{R}}{3}\left(\frac{\overline{w'q_l'S'}}{\overline{q}_l} + \frac{2\overline{w'N'S'}}{\overline{N}}\right)\right] + \overline{w'A_c'}. \tag{B3}$$

Following Stull (1988, p. 144), we can write the following budget *without* microphysics:

$$\left(\frac{\partial\overline{w'q_l'}}{\partial t}\right)_{\text{Dyn}} = -\frac{\partial\overline{w'w'q_l'}}{\partial z} - \overline{w'^2}\frac{\partial\overline{q}_l}{\partial z} + \frac{g}{\theta_0}\overline{\theta_v'q_l'} - \frac{1}{\rho_0}\overline{q_l'\frac{\partial p'}{\partial z}}. \tag{B4}$$

Adding (B3) and (B4), and including the SGS flux contribution leads to (7).

REFERENCES

Ackerman, A. S., O. B. Toon, and P. V. Hobbs, 1995: A model for particle microphysics, turbulent mixing, and radiative transfer in the stratocumulus-topped marine boundary layer and comparison with measurements. *J. Atmos. Sci.,* **52,** 1204–1236.

Albrecht, B. A., 1989: Aerosols, cloud microphysics, and fractional cloudiness. *Science,* **245,** 1227–1230.

——, M. P. Jensen, and W. J. Syrett, 1995: Marine boundary layer structure and fractional cloudiness. *J. Geophys. Res.,* **100,** 14 209–14 222.

Bott, A., T. Trautmann, and W. Zdunkowki, 1996: A numerical model of cloud-topped planetary boundary-layer: Radiation, turbulence and spectral microphysics in marine stratus. *Quart. J. Roy. Meteor. Soc.,* **122,** 635–667.

Clark, T. L., 1973: Numerical modeling of the dynamics and microphysics of warm cumulus convection. *J. Atmos. Sci.,* **30,** 857–878.

Considine, G. D., 1997: Modeling the diurnal variability in cloud

microphysics in boundary layer clouds. *J. Geophys. Res.,* **102,** 1717–1726.
Cooper, W. A., 1989: Effects of variable droplet growth histories on droplet size distributions. Part I: Theory. *J. Atmos. Sci.,* **46,** 1301–1311.
Deardorff, J. W., 1980: Stratocumulus-capped mixed layers derived from a three-dimensional model. *Bound.-Layer Meteor.,* **18,** 495–527.
Feingold, G., B. Stevens, W. R. Cotton, and R. L. Walko, 1994: An explicit cloud microphysical/LES model designed to simulate the Twomey effect. *Atmos. Res.,* **33,** 207–233.
——, ——, ——, and ——, 1998: Simulations of marine stratocumulus using a new microphysical parameterization scheme. *Atmos. Res.,* **47–48,** 505–523.
Fu, Q., S. K. Krueger, and K. N. Liou, 1995: Interactions of radiation and convection in simulated tropical cloud clusters. *J. Atmos. Sci.,* **52,** 2139–2156.
Khairoutdinov, M., and Y. Kogan, 2000: A new cloud physics parameterization in a large-eddy simulation model of marine stratocumulus. *Mon. Wea. Rev.,* **128,** 229–243.
Khvorostyanov, V. I., and J. Curry, 1999: Toward the theory of stochastic condensation in clouds. Part I: A general kinetic equation. *J. Atmos. Sci.,* **56,** 3985–3996.
Kogan, Y. L., M. P. Khairoutinov, D. K. Lilly, Z. N. Kogan, and Q. Fu, 1995: Modeling of stratocumulus clouds layers in a large-eddy simulation model with explicit microphysics. *J. Atmos. Sci.,* **52,** 2923–2940.
Lappen, C.-L., and D. A. Randall, 2001: Toward a unified parameterization of the boundary layer and moist convection. Part I: A new type of mass-flux model. *J. Atmos. Sci.,* **58,** 2021–2036.
Lilly, D. K., 1968: Models of cloud-topped mixed-layers under a strong inversion. *Quart. J. Roy. Meteor. Soc.,* **94,** 292–308.
Mellor, G. L., 1977: The Gaussian cloud model relations. *J. Atmos. Sci.,* **34,** 356–358.
Moeng, C.-H., 1986: Large-eddy simulation of a stratus-topped boundary layer. Part I: Structure and budgets. *J. Atmos. Sci.,* **43,** 2886–2900.
——, and J. C. Wyngaard, 1986: An analysis of closures for pressure-scalar covariances in the convective boundary layer. *J. Atmos. Sci.,* **43,** 2499–2513.
Nicholls, S., 1984: The dynamics of stratocumulus: Aircraft observations and comparisons with a mixed-layer model. *Quart. J. Roy. Meteor. Soc.,* **110,** 783–820.
Paluch, I. R., and D. H. Lenschow, 1991: Stratiform cloud formation in the marine boundary layer. *J. Atmos. Sci.,* **48,** 2141–2158.
Randall, D. A., 1987: Turbulent fluxes of liquid water and buoyancy in partly cloudy layers. *J. Atmos. Sci.,* **44,** 850–858.
Sigg, R., 2000: Use of pseudoadiabatic adjustment of turbulence for a simplified nighttime stratocumulus case: A one-dimensional study. *Mon. Wea. Rev.,* **128,** 2317–2328.
Sommeria, G., and J. W. Deardorff, 1977: Subgrid-scale condensation in models of nonprecipitating clouds. *J. Atmos. Sci.,* **34,** 344–355.
Squires, P., 1952: The growth of cloud drops by condensation. *Aust. J. Sci. Res.,* **A5,** 59–86.
Stevens, B., G. Feingold, W. R. Cotton, and R. L. Walko, 1996a: Elements of the microphysical structure of numerically simulated nonprecipitating stratocumulus. *J. Atmos. Sci.,* **53,** 980–1006.
——, R. L. Walko, W. R. Cotton, and G. Feingold, 1996b: The spurious production of cloud-edge supersaturation by Eulerian models. *Mon. Wea. Rev.,* **124,** 1034–1041.
——, W. R. Cotton, and G. Feingold, 1998a: A critique of one- and two-dimensional models of boundary layer clouds with a binned representations of drop microphysics. *Atmos. Res.,* **47–48,** 529–553.
——, ——, ——, and C.-H. Moeng, 1998b: Large-eddy simulations of strongly precipitating, shallow, stratocumulus-topped boundary layers. *J. Atmos. Sci.,* **55,** 3616–3638.
——, C.-H. Moeng, and P. P. Sullivan, 1999: Large-eddy simulation of radiatively driven convection: Sensitivities to the representation of small scales. *J. Atmos. Sci.,* **56,** 3963–3984.
Stull, R. B., 1988: *An Introduction to Boundary Layer Meteorology.* Kluwer Academic, 666 pp.
Telford, J. W., and S. K. Chai, 1980: A new aspect of condensation. *Pure Appl. Geophys.,* **119,** 720–742.
Twomey, S., 1977: The influence of pollution on the shortwave albedo of clouds. *J. Atmos. Sci.*, **34,** 1149–1152.
Wang, Q., H. Zuo, S. Wang, C. Zhao, and D. L. Westphal, 1998: A new turbulence closure model with explicit microphysics for marine stratocumulus. Preprints, *Conf. on Cloud Physics,* Everett, WA, Amer. Meteor. Soc., 325–328.
Wang, S., and B. Albrecht, 1986: A stratocumulus model with an internal circulation. *J. Atmos. Sci.,* **43,** 2373–2391.
——, and Q. Wang, 1994: Roles of drizzle in a one-dimensional third-order turbulence closure model of the nocturnal stratus-topped marine boundary layer. *J. Atmos. Sci.,* **51,** 1559–1576.
——, and ——, 1999: On condensation and evaporation in turbulence cloud parameterizations. *J. Atmos. Sci.,* **56,** 3338–3344.
——, and B. Stevens, 2000: Top-hat representation of turbulence statistics in cloud-topped boundary layers: A large eddy simulation study. *J. Atmos. Sci.,* **57,** 423–440.
——, and Q. Wang, 2000: A cloud microphysical parameterization for higher-order turbulence closure models. *Proc. 13th Int. Conf. on Clouds and Precipitation,* Reno, NV, ICCP, 557–560.
Wyngaard, J. C., and C.-H. Moeng, 1992: Parameterizing turbulent diffusion through the joint probability density. *Bound.-Layer Meteor.,* **60,** 1–13.
Zalesak, S. T., 1979: Fully multidimentional flux-corrected transport algorithms for fluids. *J. Comput. Phys.,* **11,** 335–362.